Journal of Power Sources 190 (2009) 301–306

Contents lists available at ScienceDirect

Journal of Power Sources

journal homepage: www.elsevier.com/locate/jpowsour

Cesium substituted 12-tungstophosphoric ($Cs_xH_{3-x}PW_{12}O_{40}$) loaded on ceria-degradation mitigation in polymer electrolyte membranes

D. Zhao[a,b], B.L. Yi[a,c,*], H.M. Zhang[a], H.M. Yu[c], L. Wang[a,b], Y.W. Ma[a,b], D.M. Xing[d]

[a] Lab of PEMFC Key Materials and Technologies, Dalian Institute of Chemical Physics, Chinese Academy of Sciences, 457 Zhongshan Road, Dalian, Liaoning 116023, PR China
[b] Graduate School of the Chinese Academy of Sciences, Beijing 100039, PR China
[c] Fuel Cell System and Engineering Laboratory, Dalian Institute of Chemical Physics, Chinese Academy of Sciences, Dalian 116023, PR China
[d] Sunrise Power Co., Ltd., Dalian 116025, PR China

ARTICLE INFO

Article history:
Received 3 December 2008
Received in revised form
25 December 2008
Accepted 30 December 2008
Available online 14 January 2009

Keywords:
Durability
12-Tungstophosphoric
Ceria
Free radicals
Peroxide
PEMFC

ABSTRACT

A novel multifunctional catalyst $Cs_xH_{3-x}PW_{12}O_{40}/CeO_2$ was prepared to mitigate the free radical attack to membranes in fuel cell environment. $Cs_xH_{3-x}PW_{12}O_{40}/CeO_2$ nanoparticles synthesized by solution-based hydrothermal method and two-step impregnation method were dispersed uniformly into the Nafion® resin, and then the composite membrane was prepared using solution-cast method. The particles prepared were characterized by X-ray powder diffraction (XRD), TEM and FT-IR to evaluate the crystallite size, distribution of the nanopaticles and the crystal structure. The membrane degradation was investigated via ex situ Fenton test and in situ open circuit voltage (OCV) accelerated test. In the durability tests, the fluoride emission rate (FER) reduced nearly one order of magnitude by adding $Cs_xH_{3-x}PW_{12}O_{40}/CeO_2$ nanoparticles into the Nafion membrane, suggesting that $Cs_xH_{3-x}PW_{12}O_{40}/CeO_2$ catalyst has a promising application to greatly improve the proton exchange membrane (PEM) durability.

1. Introduction

Proton exchange membrane fuel cells (PEMFCs) are very promising as environment-friendly energy supplier. However, their durability and cost are the key issues that should be solved for practical applications. Now the research emphasis has shifted from improving the initial performance ("beginning-of-life") to enhancing fuel cell reliability and lifetime and to making fuel cell cost competitive. Proton exchange membranes (PEMs) are the key components in fuel cell system, which limit the lifetime of the whole PEMFCs. Thus enhancement of the durability of the PEMs is critical to the lifetime and commercial viability of the PEMFCs.

In the last decade, the membrane degradation mechanism studies became the focus of attention. To sum up the recent published reports, the membrane degradations are mainly classified as chemical/electrochemical degradation and physical degradation. As for the former degradation, hydrogen peroxide and its decomposition intermediate products $HO^{\cdot}$ and $HO_2^{\cdot}$ with strong oxidative characteristics generated during the fuel cell operation have been considered as one of the important factors resulting in the membrane degradation. The formation of H_2O_2 has been confirmed using a microelectrode in an operating fuel cell [1] and detected in the outlet stream of the cell with Nafion membrane by Scherer [2]. There are two different pathways for the H_2O_2 generation and the free radical species: (1) generating at the cathode due to the electrochemical two-electron reduction of oxygen [3] or the chemical combination of crossover hydrogen and oxygen at the cathode (1)–(4) and (2) generating at the anode due to the chemical combination of crossover oxygen and hydrogen at the anode [4,5] (4)–(7).

(1) $O_2 + 2H^+ + 2e^- \rightarrow H_2O_2$
(2) $H_2O_2 + M^{2+} \rightarrow M^{3+} + HO^{\cdot} + HO^-$
(3) $HO^{\cdot} + H_2O_2 \rightarrow H_2O + HO_2^{\cdot}$ (hydrogyen peroxide radial attacks PEM)
(4) $H_2 + O_2 \xrightarrow{\text{Pt surface}} [O] + H_2O$
(5) $H_2 \rightarrow 2H^{\cdot}$ (via Pt catalyst)
(6) $H^{\cdot} + O_2$ (diffused through PEM to anode) $\rightarrow HO_2^{\cdot}$.
(7) $HO_2^{\cdot} + H^{\cdot} \rightarrow H_2O_2$ (diffused into PEM)

Effective strategies should be taken to improve the membrane durability. The passive approach is to improve polymer stability, such as synthesis of short side chain polymers [6,7], novel hydrocarbon polymer electrolytes [8], or composite membrane with PTFE

* Corresponding author at: Fuel Cell System and Engineering Laboratory, Dalian Institute of Chemical Physics, Chinese Academy of Sciences, Dalian 116023, PR China. Tel.: +86 411 84379536; fax: +86 411 84665057.
E-mail address: blyi@dicp.ac.cn (B.L. Yi).

0378-7753/$ – see front matter © 2009 Elsevier B.V. All rights reserved.
doi:10.1016/j.jpowsour.2008.12.133

[9]. The active approach is to suppress the free radicals attack, such as avoiding H_2O_2 formation, destroying H_2O_2 [10–13] or scavenging the free radicals [14,15]. Trogadas and Ramani [11] prepared Pt/C/MnO_2 hybrid catalyst to minimize the effect of reactive oxygen species at fuel cell operation condition. Though the hybrid catalyst can mitigate the generation of hydrogen peroxide, the activity of the catalysts is poor at the same time.

In this research, we designed a multifunctional catalyst which can decompose H_2O_2 and scavenge the free radicals on the surfaces of the nanoparticles. Since the scavenging catalyst is nonconductive, the cell performance may reduce with the nanoparticles dispersion. Thus, the proton conductivity was also considered. In our study, we investigated the effects of the multifunctional catalyst composed of a metal oxide with variable valence, cerium nanoparticles, and a solid acid, cesium substituted 12-tungstophosphoric, in PEMs.

CeO_2 is a metal oxide with variable valence. According to the report by Babu et al. [16], CeO_2 nanoparticles have been chosen as free radical scavenger in the biological system due to their higher surface area and ability to undergo faster redox reaction ($Ce^{3+} \leftrightarrow Ce^{4+} + e^-$). Unfortunately, CeO_2 nanoparitcles show low proton conductivity. Thus the particles with high conductivity should combine with them. Among many other solid acid systems, heteropoly acids (HPA) with Keggin anion structures have received the most attention due to their simple preparation and strong acidity [17–19]. Specifically, 12-tungstopsphoric acid ($H_3PW_{12}O_{40}$) is among the most extensively studied [20,21]. On the one hand, 12-tungstopsphoric is a stable peroxide-decomposition catalyst [22–24]. The Keggin units react with H_2O_2 and lead to the decomposition of H_2O_2 and formation of free radicals. In the fuel cell environment, the concentration of H_2O_2 are at trace level (in the order of ppm [1]), the formation of short-lifetime free radicals will be rapidly quenched by the scavengers. On the other hand, 12-tungstopsphoric possesses the highest Bönsted acidity [25], stronger than that of 100% sulfuric acid. This property can be used to improve the membrane proton conductivity. The present research is to solve the membrane degradation problem in PEMFC by preparing a multifunctional catalyst ($Cs_xH_{3-x}PW_{12}O_{40}/CeO_2$). Nafion resin is used as a model polymer material, and the influence of $Cs_xH_{3-x}PW_{12}O_{40}/CeO_2$ on the membrane degradation will be investigated in detail.

2. Experimental

2.1. Catalyst preparation

CeO_2 nanoparticles were synthesized by a solution-based hydrothermal method [26]. 1.50 g $Ce(NO_3)_3{\cdot}6H_2O$ was dissolved in 20 ml distilled water, and proper amount of 10% NaOH solution were rapidly added with stirring (keep the pH 10–12, or the particles would be dark purple). A light yellow precipitate of amorphous CeO_2 appeared. After about 10 min of stirring, all of the slurry was then transferred into a 50-ml column autoclave, which was filled with deionized water up to 70% of the total volume, and heated at 100 °C under auto-genous pressure overnight. The system was then cooled to room temperature. The final product was collected by centrifugation, washed with deionized water to remove ionic remnants, then dried at 60 °C, calcined at 350 °C for 4 h.

12-Tungstophosphoric solution was prepared using the Keggin type $H_3PW_{12}O_{40}{\cdot}H_2O$. The highly dispersed $Cs_xH_{3-x}PW_{12}O_{40}$ on CeO_2, denoted as $Cs_xH_{3-x}PW_{12}O_{40}/CeO_2$ (x = Cs stoichiometry, in our work x = 2–2.5), was prepared by using the two-step impregnation method reported by Soled et al. [17]. In the first step, 7.5 ml Cs_2CO_3 solution (0.005 M) was impregnated onto CeO_2 nanoparticals (0.2 g), dried at 110 °C overnight and calcined at 300 °C for 2 h. Following this, 4 ml $H_3PW_{12}O_{40}$ (0.008 M) was impregnated with stirring, dried at 110 °C overnight and calcined at 300 °C for 2 h. The loading of the $Cs_xH_{3-x}PW_{12}O_{40}$ on CeO_2 was about 50%. $Cs_xH_{3-x}PW_{12}O_{40}$ (x = 2–2.5) particles were also prepared as reported by Tatematsu et al. [27].

2.2. Membrane and MEA preparation

The $Cs_xH_{3-x}PW_{12}O_{40}/CeO_2$/Nafion composite membrane was prepared by the following procedure. The Nafion/DMAc solution and $Cs_xH_{3-x}PW_{12}O_{40}/CeO_2$ particles were dispersed ultrasonically to form an ink. Then the ink was poured onto a flat glass plate. The glass plate was dried on a hot plate at 60 °C for 24 h. Subsequently, the solvent was evaporated in a vacuum oven at 140 °C for 12 h. The amount of $Cs_xH_{3-x}PW_{12}O_{40}/CeO_2$ in the membrane was about 1 wt.%. The thickness of the composite membranes was about 50 μm. CeO_2/Nafion membrane was also prepared for comparison.

The Pt/C catalyst loading of the anode and the cathode are 0.3 and 0.5 mg Pt cm^{-2} respectively. Two electrodes with effective area 4 cm^2 were hot-pressed to one piece of membrane to form a MEA.

2.3. XRD, FT-IR and TEM analysis

To gather the information on the $Cs_xH_{3-x}PW_{12}O_{40}/CeO_2$ particles, the X-ray powder diffraction (XRD) analysis was performed using Panalytical X'pert PRO diffractmeter (Philps X'pert PRO) with Cu-Kα radiation source. The X-ray diffractogram was obtained for 2θ varying between 10° and 90°. The average size of the particles was calculated using Scherrer's equation as follows [28]:

$$L = \frac{0.9\lambda_{K\alpha 1}}{B_{(2\theta)}\cos\theta_{max}} \quad (1)$$

where L is the average size of the crystallites, $\lambda_{k\alpha 1}$ is the X-ray wave length (Cu-Kα, $\lambda_{k\alpha 1}$ = 1.54056 Å), θ_{max} is the angle value of the crystallite characteristic peaks, and $B_{(2\theta)}$ is the fwhm (full width at half maximum) of the diffraction line.

The infrared spectra of the membranes were recorded at a resolution of 4 cm^{-1} with a FT-IR spectrometer (JASCO FT/IR-4100). $Cs_xH_{3-x}PW_{12}O_{40}/CeO_2$ particles were recorded on a JEOL JEM-2000 microscope operated at 120 kV.

2.4. Fluorine ion determination

Fluoride emission rate (FER) was detected via ion selective electrode (ISE) [6]. It was known that the measurement was affected by sample pH values (when pH > 7, hydroxide ions will interfere with the electrode response to fluoride; for pH < 5, the proton can form a complex with a portion of the fluoride in solution by forming the undissociated acid HF and HF_2^- ions.) TISAB buffer solution (the solution made up of 500 ml deionized water, 57 ml acetic acid, 58 g NaCl and 12 g sodium citrate $Na_3C_6H_5O_7{\cdot}2H_2O$) was used to maintain the desired pH range 5–7 and good ion background. The concentration of the fluoride was measured by using standard addition method.

2.5. Linear sweep voltammetry (LSV) measurement

The crossover hydrogen and electrical shorting of the MEAs before and after the open circuit voltage (OCV) test was measured by using the linear sweep voltammetry (LSV). The cell voltage was scanned potentiodynamically at 4 mV s^{-1} in the potential range of 0–600 mV (the anode as the reference electrode) under 0.2 MPa and 80 °C with 50% RH. The potential was controlled by CHI 600B electrochemical workstation. Hydrogen crossover was determined by the plateau current density at higher potential (0.4 V), where

the current obtained was limited by the hydrogen transport rate through the membrane.

2.6. Membrane conductivity measurement

The membrane conductivity was determined by using a cell with a pair of pressure-attached copper electrodes as reported by Zawodzinski et al. [29]. The resistivity of the membrane was measured by using electrochemical impedance spectroscopy (EIS) (PARSTAT® 2273A (Princeton, USA)) electrochemical system. Signal amplitude of 20 mV in the frequency range of 1 MHz–100 Hz was applied. The sample was soaked in water at ambient temperature (20 °C) for 12 h and then sealed between two plates with electrodes. The conductivity values were calculated using

$$\sigma = \frac{L}{RS} \quad (2)$$

where σ (S cm^{-1}) is the proton conductivity of the membrane, L (cm) is the effective length of the membrane, R is the membrane resistance (Ω), and S (cm^2)is the membrane cross-sectional area. The Nyquist plots for Nafion, CeO_2/Nafion and $Cs_xH_{3-x}PW_{12}O_{40}/CeO_2$/Nafion membranes at 20 °C were shown.

2.7. Membrane durability test

The membrane durability was evaluated by both ex situ Fenton test [30] and in situ OCV accelerated test [31]. Membrane samples were respectively immersed in 50 ml Fenton solution (3 wt.% hydrogen peroxide solution and 20 ppm Fe^{2+}). The durability tests were carried out at 80 °C for 150 h. Prior to fluorine ion characterization, the Pt wire was immersed into the analyte solution to decompose the residual hydrogen peroxide, which was to assure of the accurate and reproducible results.

To characterize the membrane degradation behaviors in the fuel cell environment, the MEAs were tested at open circuit at 80 °C and 50% RH. During the test, O_2 was used as the oxidant at the cathode and H_2 was used as the fuel at the anode. The flow rate for both gases was 40 ml min^{-1} (anode) and 60 ml min^{-1} (cathode) respectively. The test ran for 24 h for each MEA, and the anode and cathode exhausted streams were independently condensed in cold-traps. The cell performance and hydrogen crossover current were also recorded.

3. Results and discussion

3.1. XRD, FT-IR and TEM characterizations

The X-ray diffraction spectrum of the $Cs_xH_{3-x}PW_{12}O_{40}/CeO_2$ shows the presence of the $Cs_xH_{3-x}PW_{12}O_{40}$ and CeO_2 in the composite particles (Fig. 1). XRD peaks that correspond to the (1 1 1), (2 0 0), (2 2 0), (3 1 1), (2 2 2), (4 0 0), (3 3 1), (4 2 0), and (4 2 2) planes of a cubic fluorite structure (space group: Fm3m) of CeO_2 as identified using the standard data JCPDS 34-0394 (Fig. 1a). The average crystallite size (D) of CeO_2 nanoparticles calculated from X-ray line broadening of the reflection of (2 2 0) using Debye-Scherrer formula is 7.4 nm [32]. The main specific diffractive peaks of different crystalline forms ($n = 2\theta$) of $Cs_xH_{3-x}PW_{12}O_{40}$ were as follows: 10.4° and 15.0°, 18.8°, 21.2°, 26.1°, 30.2° and 35.7° (Fig. 2c). This fact is consistent with the very similar lattice parameters of these salts obtained in the literature [20]. From the XRD reflection in the $Cs_xH_{3-x}PW_{12}O_{40}/CeO_2$ particles, the characteristic peaks of both $Cs_{2.5}H_{0.5}PW_{12}O_{40}$ and CeO_2 existed.

Note that the actual particle size of the $Cs_xH_{3-x}PW_{12}O_{40}/CeO_2$ nanoparticls is larger than that of CeO_2 estimated by Debye-Scherrer formula (Fig. 2), which is due to the existences of

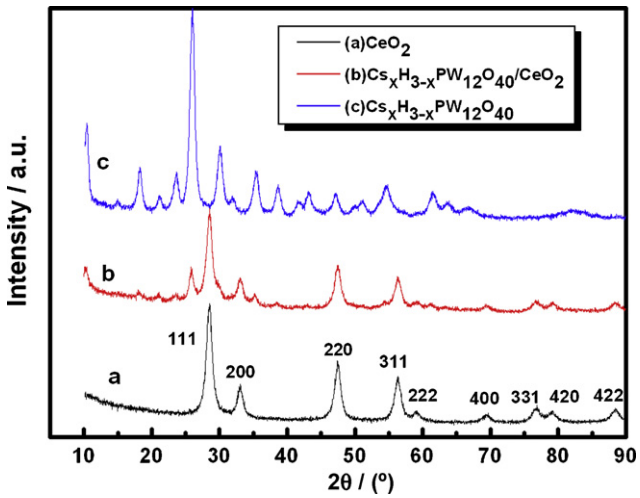

Fig. 1. X-ray diffraction scan of 50% $Cs_xH_{3-x}PW_{12}O_{40}$ loaded on CeO_2, bulk CeO_2 and $Cs_xH_{3-x}PW_{12}O_{40}$ particles.

$Cs_{2.5}H_{0.5}PW_{12}O_{40}$ and the unavoidable agglomeration in calcination process. The size of $Cs_xH_{3-x}PW_{12}O_{40}/CeO_2$ nanoparticls was approximately 12 nm and the size of agglomerates was approximately 100 nm. Furthermore, it can be seen that the $Cs_xH_{3-x}PW_{12}O_{40}$ was supported on CeO_2 in the described experimental conditions.

Fig. 3 shows the FT-IR spectra of the bulk $Cs_xH_{3-x}PW_{12}O_{40}$, CeO_2 and $Cs_xH_{3-x}PW_{12}O_{40}/CeO_2$. The four main characteristic peaks of the bulk $Cs_xH_{3-x}PW_{12}O_{40}$ are as follows: 1080 cm^{-1} (P–O in central tetrahedral), 985 cm^{-1} (terminal W=O), 890 cm^{-1} and 812 cm^{-1} and 800 cm^{-1} (W–O–W) associated with the asymmetric vibrations in the Keggin polyanion[20,33]. As for the bulk

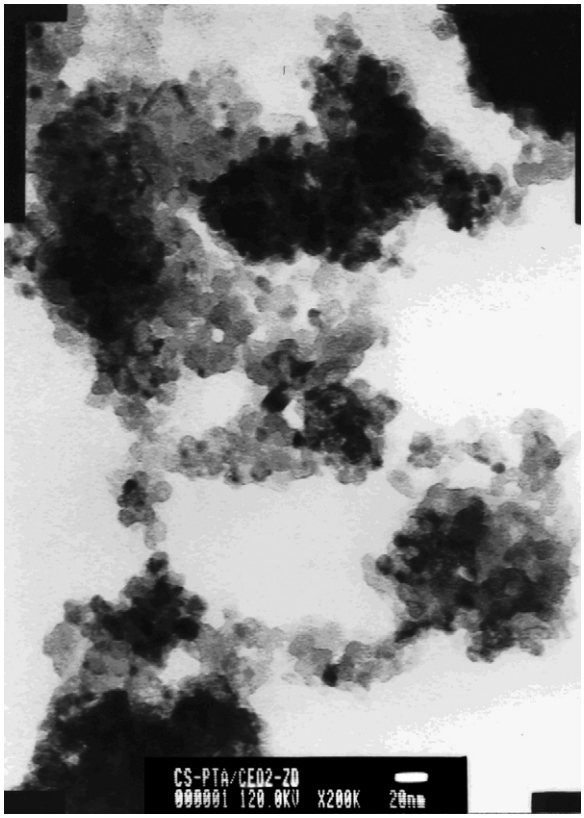

Fig. 2. TEM micrograph of $Cs_xH_{3-x}PW_{12}O_{40}/CeO_2$ nanoparticles.

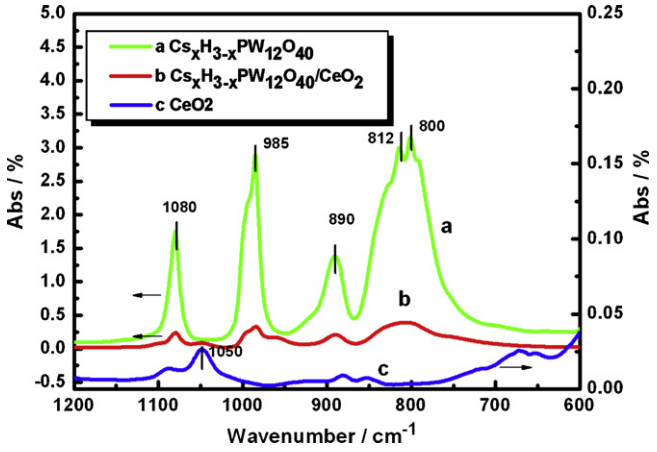

Fig. 3. FT-IR spectra of 50% $Cs_xH_{3-x}PW_{12}O_{40}$ loaded on CeO_2, bulk CeO_2 and $Cs_xH_{3-x}PW_{12}O_{40}$ nanoparticles.

CeO_2, the main peak is at 1050 cm^{-1}. It is obvious that the spectra of $Cs_xH_{3-x}PW_{12}O_{40}/CeO_2$ exhibited the characteristic peaks of $Cs_xH_{3-x}PW_{12}O_{40}$ (at 1080, 985, 890 and 812 cm^{-1}) and CeO_2 (at 1050 cm^{-1}), which indicates that the Keggin heteropoly anions $[PW_{12}O_{40}]^{3-}$ still existed in the composite nanoparticles.

3.2. Performance of PEMFCs operated at 50% RH condition

As it is known that CeO_2 are non-electric conductive particles, the addition of CeO_2 will impact the membrane proton conductivity. Thus we designed to prepare the composite particles $Cs_xH_{3-x}PW_{12}O_{40}/CeO_2$ to compensate this defect. 12-tungstopsphoric acid is Bönsted acidity [25], which is stronger than that of 100% sulfuric acid. As reported by Wang [33], H^+ in the 12-tungstopsphoric acid was partly substituted by Cs^+, thus the $Cs_{2.5}H_{0.5}PW_{12}O_{40}/CeO_2$ was steady in the aqueous condition and the conductivity of the membrane was improved. Fig. 4 shows the polarization curves of the cells with Nafion, CeO_2/Nafion and $Cs_xH_{3-x}PW_{12}O_{40}/CeO_2$/Nafion membranes operated at 50% RH condition with the cell temperature at 80 °C respectively. The cell performance with $Cs_xH_{3-x}PW_{12}O_{40}/CeO_2$/Nafion membrane was better than that with CeO_2/Nafion membrane, and similar to that of Nafion membrane. As shown in Fig. 5, the resistance of $Cs_xH_{3-x}PW_{12}O_{40}/CeO_2$ membrane was much lower than CeO_2/Nafion membrane, thus the membrane conductivity was greatly improved by dispersing $Cs_xH_{3-x}PW_{12}O_{40}/CeO_2$ nanoparticles into the membrane.

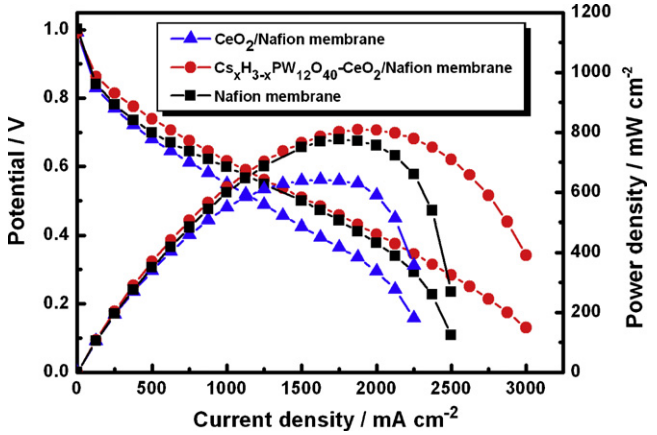

Fig. 4. Fuel cell performance of Nafion, CeO_2/Nafion and $Cs_xH_{3-x}PW_{12}O_{40}/CeO_2$/Nafion membranes at 80 μm, 50% RH condition.

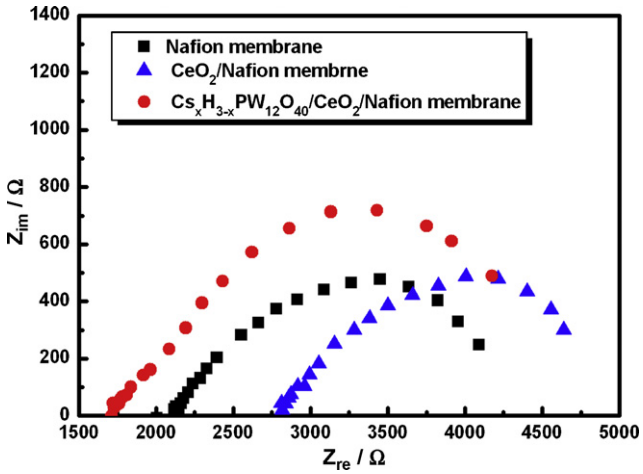

Fig. 5. The Nyquist plots for Nafion, CeO_2/Nafion and $Cs_xH_{3-x}PW_{12}O_{40}/CeO_2$/Nafion membranes at 20 °C.

3.3. Membrane durability test

3.3.1. Ex situ Fenton test results—fluoride emission rate (FER)

The FER of the membranes showed the chemical durability of the sample membranes at this test condition (3 wt. % hydrogen peroxide solution and 20 ppm Fe^{2+}, at 80 °C). Two conclusions can be readily drawn from an inspection of Fig. 6: (1) The addition of CeO_2 and $Cs_xH_{3-x}PW_{12}O_{40}/CeO_2$ particles resulted in a great reduction in the FER. (2) Compared to CeO_2/Nafion composite membrane, the FER was much lower with the $Cs_xH_{3-x}PW_{12}O_{40}/CeO_2$ particles dispersing into the membrane.

CeO_2 nanoparticles have already been shown to be an excellent free radical scavenger in biological systems [34]. Moreover, the oxygen free radical ($HO^{\bullet}$, $HO_2^{\bullet}$) scavenging property of CeO_2 nanoparticles was confirmed by using electron paramagnetic resonance (EPR) technique with the presence of a spin trap DMPO (5,5-dimethylpyrroline-*N*-oxide) [16]. This property mentioned above was due to the high thermodynamic affinity for oxygen and the relative ease to undergo reversible redox reaction between Ce^{3+} and Ce^{4+} state. McGinnis and co-workers [35] had shown that reducing the diameter of CeO_2 nanoparticles resulted in more oxygen vacancies, which made them even better scavengers. The increased surface area to volume ratio of CeO_2 nanoparticles enabled them to regenerate their scavenging activities. The free radical scavenging process was as follows:

$$Ce^{3+} \leftrightarrow Ce^{4+} + e^-$$

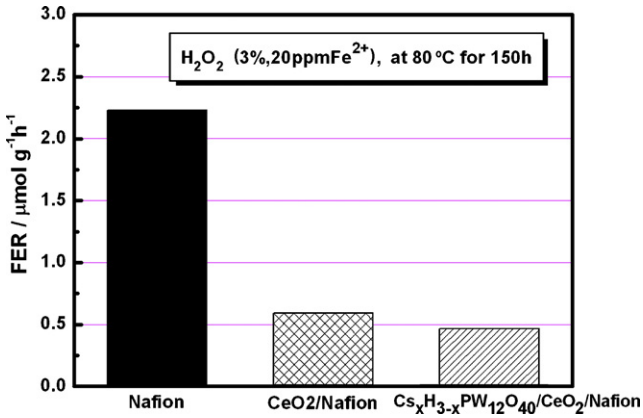

Fig. 6. Fluoride emission rate (FER) of Nafion membrane and composite membrane with CeO_2 and $Cs_xH_{3-x}PW_{12}O_{40}/CeO_2$ nanoparticles in Fenton test.

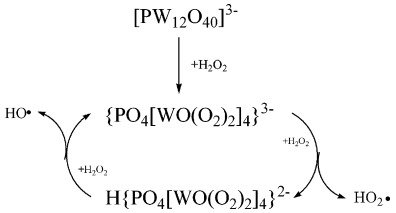

Scheme 1. The H_2O_2 decomposition catalyzed by Keggin heteropoly anions $[PW_{12}O_{40}]^{3-}$ and $\{[PO_4[WO(O_2)_2]_4\}^{3-}$.

$$Ce^{3+} + HO^{\bullet} \rightarrow Ce^{4+} + OH^{-}$$

On the other hand, $Cs_xH_{3-x}PW_{12}O_{40}$ is likely an effective catalyst for H_2O_2 decomposition. The FT-IR results showed that the Keggin heteropoly anions $[PW_{12}O_{40}]^{3-}$ still existed in these composite particles. As reported by Huang et al. [22], phosphotungstic acid with Keggin unit, which was a solid super acid, completely decomposed to H^+ and $[PW_{12}O_{40}]^{3-}$ in aqueous solution and reacted with H_2O_2 leading to the decomposition of H_2O_2 and formation of free radicals. These heteropoly anions, $[PW_{12}O_{40}]^{3-}$, reacted with H_2O_2 and produced another heteropoly anion, $\{[PO_4[WO(O_2)_2]_4\}^{3-}$, as shown in the following equation:

$$[PW_{12}O_{40}]^{3-} + 8H_2O_2 \rightarrow \{PO_4[WO(O_2)_2]_4\}^{3-} + 8H_2WO_4 \quad (3)$$

$\{PO_4[WO(O_2)_2]_4\}^{3-}$ reacted with H_2O_2 continually and led to the rapid formation of hydroxyl radical ($HO^{\bullet}$) and hydroperoxide radical ($HO_2^{\bullet}$) [36], as shown in Scheme 1, Subsequently, the byproducts ($HO^{\cdot}$ and $HO_2^{\cdot}$) will be rapidly scavenged by CeO_2 particles, where $Cs_xH_{3-x}PW_{12}O_{40}$ is loaded. Thus the composite particles can reduce the concentration of the H_2O_2 around the membrane bulk. The conceptual model of the scavenging process was shown in Scheme 2, which explained the reason that $Cs_xH_{3-x}PW_{12}O_{40}/CeO_2$ particles was more effective than bulk CeO_2 particles to improve the membrane durability in Fenton reagent.

3.3.2. *In situ OCV accelerated test results*

Three cells with different MEAs were tested,

(1) MEA 1# with Nafion membrane,
(2) MEA 2# with CeO_2/Nafion composite membrane,
(3) MEA3# with $Cs_xH_{3-x}PW_{12}O_{40}/CeO_2$/Nafion membrane.

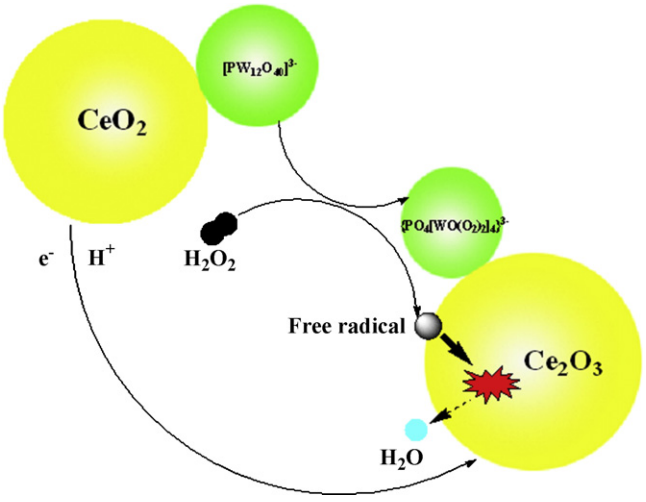

Scheme 2. The conceptual model of the scavenging process by $Cs_xH_{3-x}PW_{12}O_{40}/CeO_2$ nanoparticles.

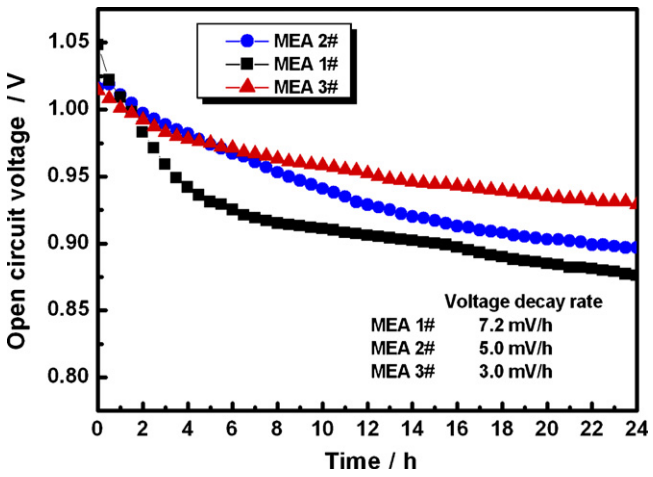

Fig. 7. Durability comparison of different MEAs in OCV test.

In all the three cases the cell was kept at 80 °C, 50% RH and the cells were left at OCV condition. As it can be observed in Fig. 7, which showed the degradation of the membrane by measuring the decay of the open circuit voltage, the voltage decay rate of MEA 3# is smaller than the others. Further more, the hydrogen crossover monitored by LSV (Fig. 8) showed that before the OCV test, the limiting currents of the three MEAs were lower than 3 mA cm^{-2}, and after 24 h OCV test, the Nafion membrane (cast) behaved a higher limiting current than the others, which indicated that a serious hydrogen crossover took place in MEA 1# [37]. Meanwhile, the addition of CeO_2 and $Cs_xH_{3-x}PW_{12}O_{40}/CeO_2$ catalysts resulted in a greater reduction (especially the $Cs_xH_{3-x}PW_{12}O_{40}/CeO_2$ catalysts makes an order of magnitude reduction) in the FER of each electrode (Fig. 9). Compared with the result from ex situ Fenton test, the scavengers were much more effective at the in situ fuel cell condition. That is because the concentration of H_2O_2 is at trace level (in the order of ppm [1]) in the cell environment, and the formation of free radicals will be rapidly quenched by the scavengers.

These results indicated that the addition of CeO_2 and $Cs_xH_{3-x}PW_{12}O_{40}/CeO_2$ catalysts reduced the membrane degradation caused by peroxide and free radicals attack at fuel cell condition. The conceptual model of the scavenging process at the in situ fuel cell condition was shown in Scheme 3, which explained the reason of the membrane durability improvement by $Cs_xH_{3-x}PW_{12}O_{40}/CeO_2$ nanoparticles.

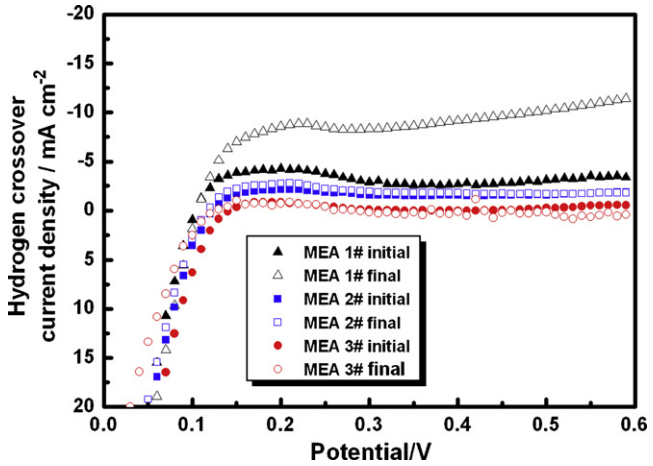

Fig. 8. Comparison of hydrogen crossover with different MEAs at the beginning and end of the OCV test.

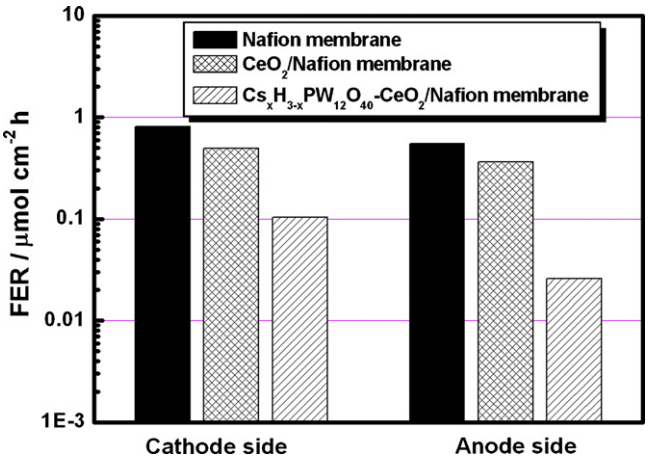

Fig. 9. FER measurement for three membranes during OCV accelerated durability test.

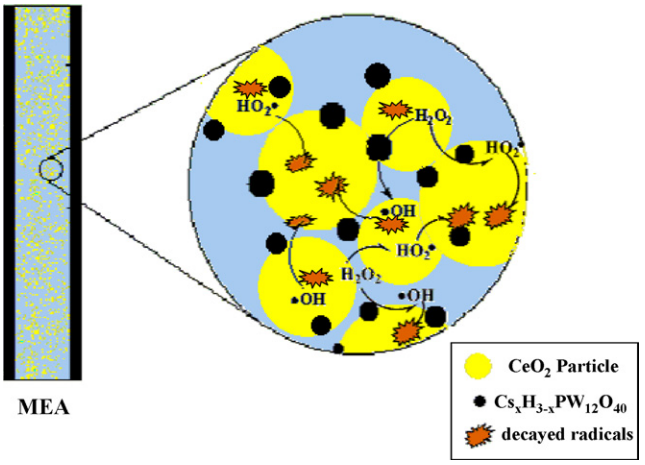

Scheme 3. The conceptual model of the in situ scavenging process at fuel cell condition.

4. Conclusions

A multifunctional catalyst $Cs_xH_{3-x}PW_{12}O_{40}/CeO_2$ ($x = 2–2.5$) as oxygen free radical ($HO^•$, $HO_2^•$) scavenger was prepared and the scavenging mechanism was discussed. The particles prepared were characterized by XRD, TEM and FT-IR to determine the crystallite size and structure, as well as the distribution of the nanopaticles. The addition of $Cs_xH_{3-x}PW_{12}O_{40}/CeO_2$ improved the conductivity of the PEM compared with CeO_2, and the performance of the cell with $Cs_xH_{3-x}PW_{12}O_{40}/CeO_2$/Nafion membrane was similar to that of Nafion membrane. The durability of the composite membranes was evaluated via Fenton test and OCV accelerated test. $Cs_xH_{3-x}PW_{12}O_{40}$ particles can decompose H_2O_2 around the membrane bulk, and as a metal oxide with variable valence, CeO_2 can quench the free radicals effectively. FER and LSV measurements obtained during the durability tests revealed that the addition of $Cs_xH_{3-x}PW_{12}O_{40}$ to the PEM can mitigate the degradation of the membrane polymer material. It is suggested that the metal oxides with variable valence, which are relative ease to undergo reversible redox reaction between M^{n+} and $M^{(n+1)+}$ state, and to make the H_2O_2 decomposition thermodynamically possible in acidic media, were promising to mitigate the degradation of PEMs.

Acknowledgment

We greatly acknowledge the financial support from National Natural Science Foundation of China (20636060).

References

[1] W. Liu, D. Zuckerboard, J. Electrochem. Soc. 152 (2005) A1165–A1170.
[2] G.G. Scherer, Ber. Bunsen-Ges, Phys. Chem. 94 (1990) 1008–1014.
[3] Q. Guo, P.N. Pintauro, H. Tang, S. O'Connor, J. Membr. Sci. 154 (1999) 175–181.
[4] F.N. Buchi, B. Gupta, O. Haas, G.G. Scherer, Electrochim. Acta 40 (1995) 345–353.
[5] J. Xie, D.L. Wood, D.M. Wayne, T.A. Zawodzinski, P. Atanassov, R.L. Borup, J. Electrochem. Soc. 152 (2005) A104–A113.
[6] C. Zhou, M.A. Guerra, Z.M. Qiu, T.A. Zawodzinski Jr., D.A. Schiraldi, Macromolecules 40 (2007) 8695–8707.
[7] L. Merlo, A. Ghielmi, L. Cirillo, M. Gebert, V. Arcella, J. Power Sources 171 (2007) 140–147.
[8] M. Aoki, N. Asano, K. Miyatake, H. Uchida, M. Watanabe, J. Electrochem. Soc. 153 (2006) A1154–A1158.
[9] S. Kundu, M.W. Fowler, L.C. Simon, R. Abouatallah, N. Beydokhti, J. Power Sources 183 (2008) 619–628.
[10] D.M. Xing, H.M. Zhang, L. Wang, Y.F. Zhai, B.L. Yi, J. Membr. Sci. 296 (2007) 9–14.
[11] P. Trogadas, V. Ramani, J. Power Sources 174 (2007) 159–163.
[12] M. Aoki, H. Uchida, M. Watanabe, Electrochem. Commun. 8 (2006) 1509–1513.
[13] H. Xu, X. Hou, Int. J. Hydrogen Energy 32 (2007) 4397–4401.
[14] A.B. LaConti, M. Hamdan, R.C. McDonald, in: W. Vielstich, H.A. Gasteiger, A. Lamm (Eds.), Handbook of Fuel Cells—Fundamentals, Technology, Applications, John Wiley & Sons, 2003, p. 659.
[15] P. Trogadas, J. Parrondo, V. Ramani, Electrochem. Solid State Lett. 11 (7) (2008) B113–B116.
[16] S. Babu, A. Velez, K. Wozniak, J. Szydlowska, S. Seal, Chem. Phys. Lett. 442 (2007) 405–408.
[17] S. Soled, S. Miseo, G. McVicker, W.E. Gates, A. Gutierrez, J. Paes, Catal. Today 36 (1997) 441–450.
[18] I.V. Kozhevnikov, Catal. Rev. Sci. Eng. 37 (2) (1995) 311–352.
[19] S. Choi, Y. Wang, Z. Nie, J. Liu, C.H.F. Peden, Catal. Today 55 (2000) 117–124.
[20] G.D. Yadav, N.S. Asthana, V.S. Kamble, J. Catal. 217 (2003) 88–99.
[21] A. Corma, Chem. Rev. 95 (1995) 559–614.
[22] Q. Huang, S. Wang, J. Huang, L. Zhuo, Y. Guo, Carbohydr. Polym. 68 (2007) 761–765.
[23] Q. Huang, L. Zhuo, Y. Guo, Carbohydr. Polym. 72 (2008) 500–505.
[24] D. Huang, Y.J. Wang, L.M. Yang, G.S. Luo, Ind. Eng. Chem. Res. 45 (2006) 1880–1885.
[25] M. Misono, N. Mizuno, K. Katamura, A. Kasai, Y. Konishi, K. Sakata, T. Okuhara, Y. Yoneda, Bull. Chem. Soc. Jpn. 55 (1982) 400–406.
[26] K. Zhou, X. Wang, X. Sun, Q. Peng, Y. Li, J. Catal. 229 (2005) 206–212.
[27] S. Tatematsu, T. Hibi, T. Okuhara, M. Misono, Chem. Lett. (1984) 865–868.
[28] V. Radmilovic, H.A. Gasteiger, P.N. Ross Jr., J. Catal. 154 (1995) 98–106.
[29] T.A. Zawodzinski Jr., M. Neeman, L.O. Sillerud, S. Cottesfeld, J. Phys. Chem. 95 (1991) 6040–6044.
[30] J. Qiao, M. Saito, K. Hayamizu, T. Okadaz, J. Electrochem. Soc. 153 (6) (2006) A967–A974.
[31] K. Teranishi, K. Kawata, S. Tsushima, S. Hirai, Electrochem. Solid State Lett. 9 (10) (2006) A475–A477.
[32] C. Li, N. Sun, J. Ni, J. Wang, H. Chu, H. Zhou, M. Li, Y. Li, J. Solid State Chem. 181 (2008) 1298–1306.
[33] L. Wang, B.L. Yi, H.M. Zhang, D.M. Xing, Electrochim. Acta 52 (2007) 5479–5483.
[34] D. Schubert, R. Dargusch, J. Raitano, S.W. Chan, Biochem. Biophys. Res. Commun. 342 (2006) 86–91.
[35] S. Deshpande, S. Patil, S. Kuchibhatla, S. Seal, Appl. Phys. Lett. 87 (2005) 133113.
[36] R. Neumann, M. de la Vega, J. Mol. Catal. 84 (1993) 93–108.
[37] J. Yu, T. Matsuura, Y. Yoshikawa, M.N. Islam, M. Hori, Electrochem. Solid State Lett. 8 (3) (2005) A156–A158.